RSC Advances

PAPER

View Article Online
View Journal | View Issue

Cite this: *RSC Adv.*, 2025, **15**, 23681

Effects of diphenyl-vinyl-substituted diketopyrrolopyrrole isomers on stacking and luminescence†

Ruixin Wang, Puxi Yang, Huizhi Chen, Songming Lan, Haoyu Li, Wei Fan,* Guangpeng Gao* and Xiaofang Li*

Received 3rd June 2025
Accepted 2nd July 2025

DOI: 10.1039/d5ra03935e

rsc.li/rsc-advances

Two kinds of novel diphenyl-vinyl-substituted diketopyrrolopyrrole derivatives with different configurations, linear shaped **R-4DPs** *vs.* S shaped **R-2DPs**, were synthesized and characterized to explore their structural, optical, and electrochemical properties. The distinct placement of diphenyl significantly affected molecular planarity, conjugation and π–π stacking in the solid state, as confirmed by single-crystal X-ray diffraction analysis. The layer spacing of compounds with 4-diphenyl were approximately 3.30–3.40 Å. These molecules exhibited strong absorption in the visible region (350–680 nm) and emitted magenta fluorescence in solution, whereas 4-diphenyl-substituted derivatives (**R-4DPs**) displayed more intense absorption and redshift attributed to enhanced conjugation with linear and rigid configuration.

Introduction

Conjugated organic materials with precisely engineered molecular packing exhibit exceptional optoelectronic properties, making them indispensable for next-generation devices.[1] The strategic control of intermolecular arrangements—particularly through π–π stacking, J/H-aggregation, and crystalline domain alignment—directly governs critical performance metrics in the organic electronics, including organic light-emitting diodes (OLEDs),[2] organic solar cells (OSCs),[3] and organic field-effect transistors (OFETs).[4] Among these materials, diketopyrrolopyrrole (DPP)-based derivatives represent a leading class of organic semiconductors, offering tunable electronic structures and exceptional photophysical properties through precisely engineered solid-state packing achieved *via* side-chain design and packing control.[5] The DPP core, characterized by its strong electron-withdrawing ability and planar aromatic structure, facilitates efficient π–π stacking and intermolecular charge transport, making it an ideal building block for designing advanced organic semiconductors.

DPP-based conjugated small molecules or polymers incorporating vinyl groups have been extensively investigated, demonstrating notable advantages such as extended conjugation length, broadened long-wavelength absorption, enhanced planarity, intermolecular interactions and high hole/electron carrier mobility,[6] thereby enhancing their suitability for phototheranostic,[7] charge transfer[8] or other applications.[9] In this study, we report the synthesis and characterization of a series of diphenyl-vinyl-substituted DPP derivatives (**R-*n*DPP-DPPs**, R = alkyl, *n* = substituent position of diphenyl, DPP may be omitted for clarity to give the name of **R-*n*DPPs**). The **R-4DP** isomers displayed valence bond conjugation with larger degree of red shift, and strong donor–acceptor (D–A) interactions,[10] as well as their absorption and fluorescence properties,[11] they also showed highly planar molecular geometry, rigidity and tight π–π stacking. The **R-2DP** isomer mainly manifested as space interaction, distorted molecular structure and caged packing, maintained strong fluorescence with large amount of bad solvent. Except for solubility, the N-substituents also affect the packing pattern.

Results and discussion

Four **R-*n*DP** derivatives were successfully synthesized with moderate yields, which were performed applying the methodology discovered by Scott and co-workers.[12] The initial step involved the reaction of fumaryl chloride with *n*-butylamine or 2-ethylhexylamine to afford the corresponding fumaramides. The key intermediate **Me-DPP** was subsequently synthesized through a sequential process involving amidation with isopropenyl acetate followed by intramolecular cyclization. A pursuant Knoevenagel condensation was employed to introduce vinylene bridges, facilitating the conjugation of various aryl moieties and resulting in the target compounds: **R-*n*DPPs**

Key Laboratory of Cluster Science of Ministry of Education, Beijing Key Laboratory of Photoelectronic/Electrophonic Conversion Materials, School of Chemistry and Chemical Engineering, Beijing Institute of Technology, Beijing 100081, P. R. China. E-mail: guangpeng008@bit.edu.cn

† Electronic supplementary information (ESI) available. CCDC 2424107–2424109. For ESI and crystallographic data in CIF or other electronic format see DOI: https://doi.org/10.1039/d5ra03935e

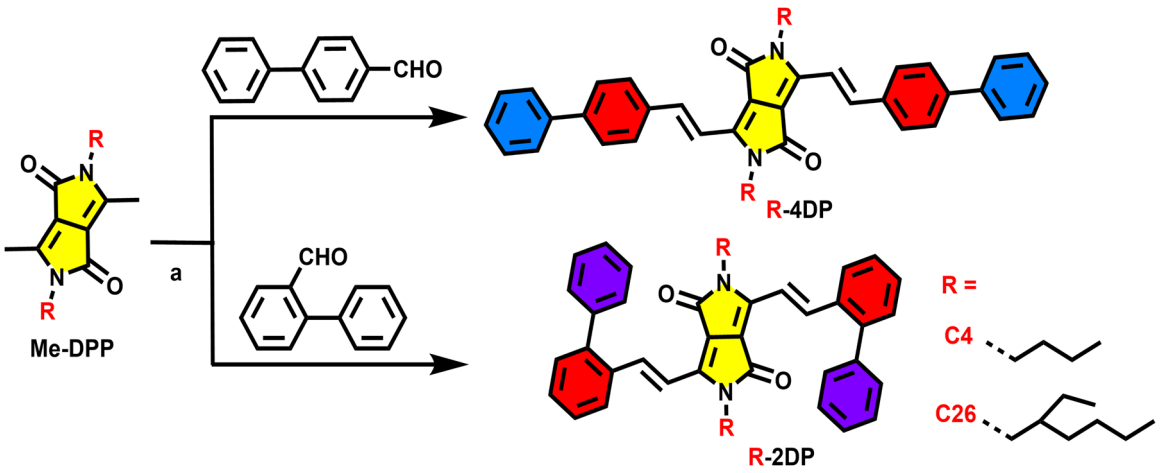

Scheme 1 Synthetic route of all R-*n*DPs. (a) Piperidine, acetonitrile, 80 °C, yield in 82–87%.

(Scheme 1). These compounds exhibited favourable solubility/dispersibility in common organic solvents (*e.g.*, dichloromethane, chloroform, toluene).

The crystallographic structures of **C4-4DP**, **C26-4DP** and **C4-2DP** were unambiguously established through single-crystal X-ray diffraction analysis, and the crystallographic data were summarized in Table S1.† But **C26-2DP** showed a bituminous appearance with no crystalline appearance at room temperature. As shown in Fig. 1a, the **C4-4DP** exhibited a highly planar configuration with a linear molecular architecture, demonstrating an end-to-end distance of 2.47 nm. The dihedral angle between the two adjacent benzene rings was 23.43°, and the dihedral angle between the B-benzene ring and the DPP core was 9.52° (Table S2†). The lengths of intramolecular hydrogen bonds were 2.33–2.37 Å, while that of intermolecular hydrogen bonds were 2.40–2.48 Å. The bond lengths analysis revealed a characteristic alternation between single and double bonds within both the DPP core and benzene rings, consistent with the electronic delocalization typical of aromatic systems. The crystal packing revealed an X-type stacking mode, the angels of two diphenyl were about 14.72° and 13.67° (α_1 and α_3), the angel of two DPP cores was about 55.25° (α_1 and α_2). The interlayer π–π distance was about 3.40 Å with a dihedral angle of 5.18° between adjacent DPP molecules (Fig. 2).

Compared to **C4-4DP**, **C26-4DP** showed similar skeletal features but exhibited unique characteristics in terms of planarity and stacking, affected by side chain (Fig. 1b). The B-benzene ring was almost coplanar to the DPP core, with a dihedral angle of only 2.57°. However, there was a significant torsion angle of 37.11° between the A and B benzene rings due to the steric hindrance, and the overall molecular length was about 2.46 nm. The different layers of **C26-4DP** were parallel to each other and slip slightly, with a layer spacing of approximately 3.30 Å (Fig. S1 and Table S2†).

For **C4-2DP**, the molecular geometry highly twisted as S shape, with a molecular width about 1.36 nm, and the angle between adjacent molecules was 86.92°, approaching a nearly perpendicular arrangement (Fig. 1c and S2†). Four molecules enclosed in a cage accumulation. The dihedral angle between the B-benzene ring and the DPP core was 34.11°, while the

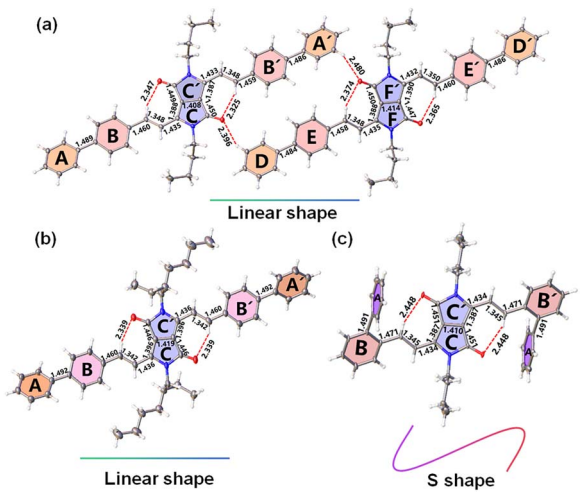

Fig. 1 Crystal structures of (a) **C4-4DP**, (b) **C26-4DP** and (c) **C4-2DP**. ORTEP drawings of the molecular structures (ellipsoid probability of 50%) with partial bond lengths in front view.

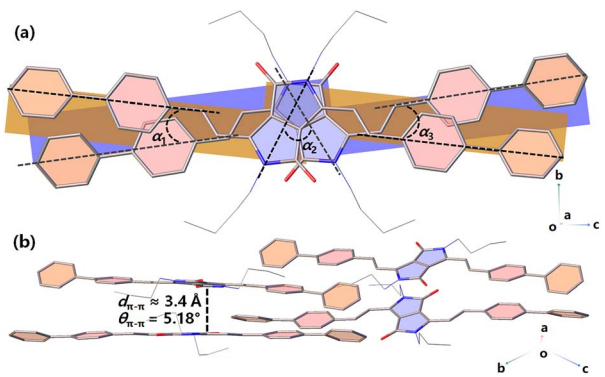

Fig. 2 Molecular packing of **C4-4DP** from (a) front view and (b) top view.

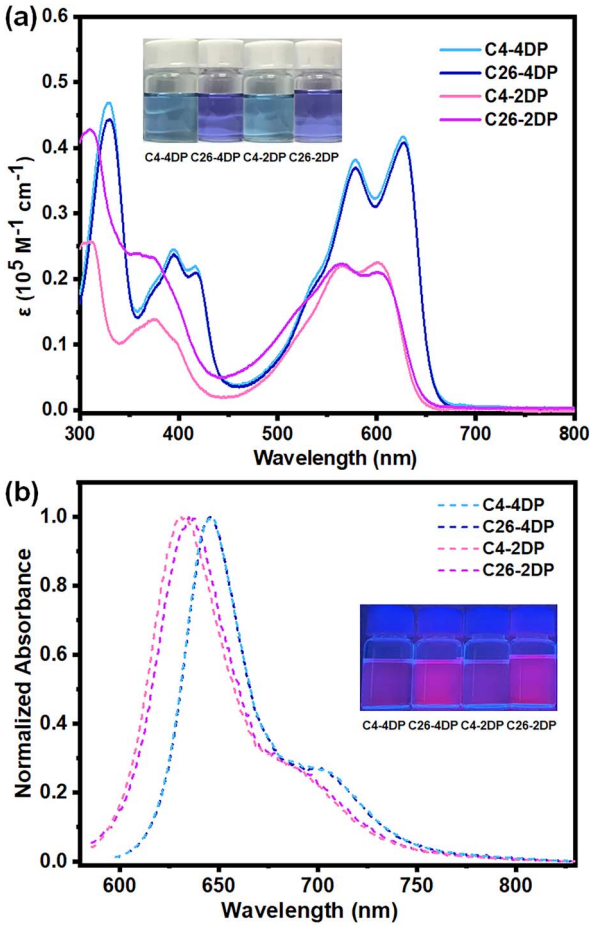

Fig. 3 Absorption and emission spectra of all R-*n*DPs in solution ($CHCl_3$, 1.0 × 10^{-5} M). (a) UV-vis absorption spectra, with an inset showing the colour of the solution under daylight; (b) normalized photoluminescence (PL) spectra, with an inset showing the colour of the solution under 365 nm UV lamp.

dihedral angle between A and B benzene rings was 89.92°, almost perpendicular to each other (Table S2†). The length of intramolecular hydrogen bonds was around 2.45 Å. Due to the highly twisted conformation, the distance of layer spacing was approximately 7.90 Å, without π–π interactions between the adjacent layer molecules.

Fig. 3 and Table 1 displayed the optical spectra and relative data of all **R-*n*DPs**, respectively. These compounds showed wide absorption with a range of 300–680 nm. **R-4DPs** exhibited strong absorbance and donor–acceptor (D–A) effect due to the stronger conjugation effect, which leading to significant redshift, with two main absorption peaks at 578 nm and 627 nm, respectively, appearing blue in solution phase and deep purple in solid state (Fig. S3†). The solutions exhibited intense red fluorescence, with a maximum emission peak at 646 nm. Due to the twisted molecular structures, **R-2DPs** showed smaller redshift, with main absorption peaks around 566 nm and 602 nm. The compounds exhibited purple coloration in solution and deep red pigmentation in the solid state, with longer Stokes shifts and a maximum emission peak around 635 nm. All four compounds exhibited fluorescence lifetimes shorter than 2 ns in solution phase (Fig. S4†). Additionally, the solvent dependence studies of **C26-4DP** and **C26-2DP** using UV-visible spectrophotometry showed minimal variation (Fig. S5†).

Fig. S6† showed the optical absorption and emission spectra of the non-annealed films of **R-*n*DPs** derivatives, indicating a collective preference for long-wavelength absorption in solid state. The dominant bands of the four substances exhibited significant redshifts compared to their solution spectra. Among them, **R-4DPs** had maximum emission peaks at 646 nm and 702 nm. These noticeable and broad spectral changed stem from the close distance (approximately 3.3 Å) and strong electronic coupling interactions due to π–π stacking in the solid state. In contrast, **R-2DPs** showed no obvious Davydov components due to more flexible conjugation.

The photoluminescence dependent aggregation assay was recorded for **C4-4DP** and **C4-2DP** in THF/H_2O mixtures (Fig. 4). As H_2O added into THF, both exhibited typical aggregation-caused quenching (ACQ) behaviour. The maximum emission wavelength (λ_{emi}) of **C4-4DP** appeared at 646 nm, and its intensity decreased with increasing water fraction (f_w), almost quenching over 60%, which mainly caused by the high degree of molecular planarity and aggregation. However, **C4-2DP** showed an emission peak (λ_{emi}) at 634 nm, and the PL intensity of **C4-4DP** was still obvious with water fraction of 80%, due to twisted structure relative to the *ortho*-isomer.

The electrochemical properties of these compounds were tested *via* cyclic voltammetry, revealing clear oxidation and reduction onset potentials (Fig. S7a and b†). Specifically, the onset reduction potentials of **C4-4DPs** and **C4-2DPs** were

Table 1 Optical data for all R-*n*DPs

	UV-vis[a]										
	λ_{max}^{liqu} (nm)	ε_{max} (M^{-1} cm^{-1})	λ_{max}^{film} (nm)	λ_{emi}^{liqu}[b] (nm)	λ_{emi}^{film} (nm)	Stokes $shift^{liqu}$ (nm)	Stokes $shift^{film}$ (nm)	Φ^{liqu}[c] (%)	Φ^{film} (%)	τ (ns)	E_g^{opt} (eV)
C4-4DP	578/627	38 200/41 700	600/656	646	695	20	39	10.9	0.6	1.256	1.90
C26-4DP	578/627	36 900/40 800	594/650	646	688	19	38	12.3	0.3	1.303	1.89
C4-2DP	563/600	22 000/22 500	578/622	634	657	34	35	10.8	0.3	1.588	1.94
C26-2DP	566/602	22 300/21 000	572/614	635	651	33	36	11.2	0.5	1.659	1.93

[a] The photophysical properties of the compounds were measured in $CHCl_3$ (1.0 × 10^{-5} M); E_g^{opt} is the optical band gap and estimated from the onset of the absorption peak, ($E_g^{opt} = 1240/\lambda_{onset}$). [b] Measured in dilute $CHCl_3$ solution. [c] Determined by absolute quantum yield in $CHCl_3$ (1.0 × 10^{-5} M).

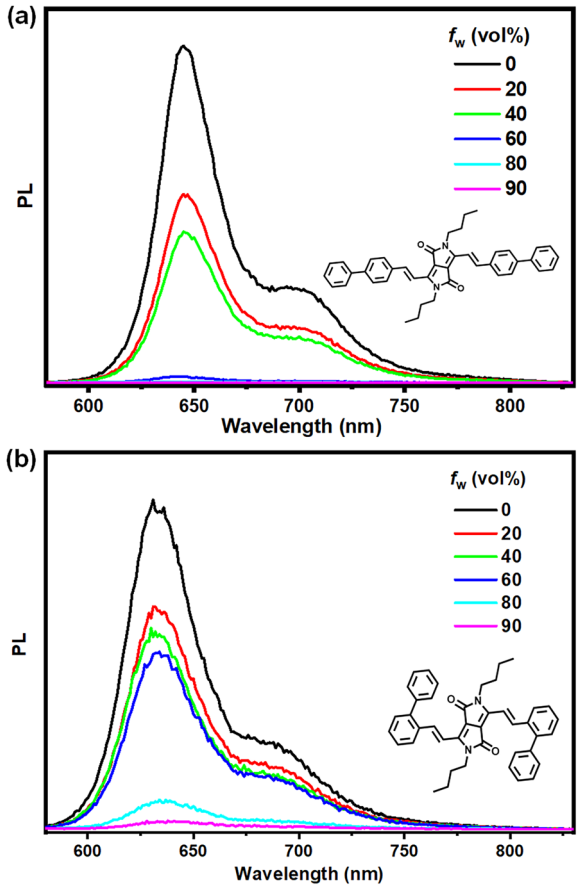

Fig. 4 (a) Fluorescence emission spectra of C4-4DP in different ratios of THF/H_2O; (b) fluorescence emission spectra of C4-2DP in different ratios of THF/H_2O. f_w Represents water fraction.

approximately −0.72 V and −0.79 V, respectively, while the onset oxidation potentials were approximately −0.92 V and 0.89 V, respectively. The former had lower LUMO energy level and narrower energy gaps; this phenomenon was consistent with the compounds with alkyl chain of ethylhexyl.

The optimized geometric configurations, highest occupied molecular orbitals (HOMO), and lowest unoccupied molecular orbitals (LUMO) energies of the compounds were determined computationally at the B3LYP/6-31G(d) level of theory within the framework of density functional theory (DFT), as shown in Fig. 5a and b. The energy gaps of **R-4DPs** were 2.12 eV, lower than that of **R-2DPs** (2.24 eV), which was consistent with different conjugation modes. Time-dependent DFT calculations based on the B3LYP/6-31G(d) level estimated the lowest absorption peaks of **R-4DP** and **R-2DP** to be 645 nm and 604 nm, respectively, corresponding to the HOMO–LUMO transitions (Fig. S7c†), which were basically consistent with the experimental values. To further explore the relationship between chemical structure and intermolecular interactions, electrostatic potential distribution (ESP) analyses of **R-*n*DPs** were conducted (Fig. 5c). Notably, all molecular surfaces exhibited positive ESP values, indicating their characteristics as electron acceptors.

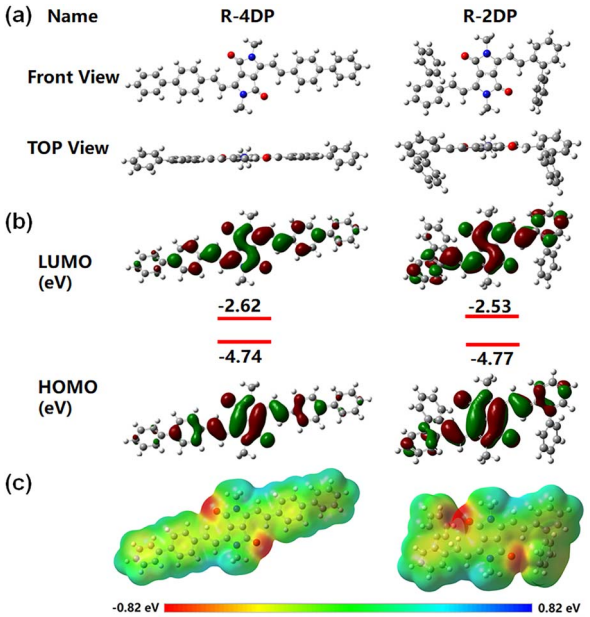

Fig. 5 At the B3LYP/6-31g(d) level, DFT calculations were performed for (a) the optimized geometric configurations in both front and top views for all R-*n*DPs, (b) HOMO and LUMO energies, and (c) electrostatic potential surfaces. To simplify the calculations, methyl groups were substituted at the imine positions for 2-ethylhexyl and *n*-butyl groups.

Conclusions

In conclusion, a series of diphenyl-vinyl-substituted DPP derivatives were successfully synthesized and comprehensively characterized to investigate their structural, optical, and electrochemical properties. The incorporation of diphenyl-vinylene significantly influenced molecular geometry, packing, and D–A interactions, optoelectronic behaviour. Single-crystal X-ray diffraction revealed distinct packing motifs, with **R-4DPs** exhibiting planar structure and strong π–π interactions, while **C4-2DP** displayed a twisted conformation with cage-shaped stacking. Optical studies demonstrated that the **R-*n*DPs** exhibited strong absorption in the visible region and fluorescence in solution, with notable redshift in thin films due to intermolecular interactions. **R-4DPs** exhibited strong absorbance and significant redshift due to stronger conjugation effect, meanwhile, **C4-2DP** maintained PL intensity mightily upon high fraction of H_2O in THF due to twisted structures. This study underscores the potential of **R-*n*DPs** as promising candidates for organic semiconductors in optoelectronic devices and provides a foundation for the rational design of conjugated materials with tailored properties for future applications. The related applications about fluorescence imaging or photothermal therapy is undergoing in our laboratory.

Data availability

Crystallographic data for the structures reported in this article have been deposited at the Cambridge Crystallographic Data Centre, under deposition numbers CCDC 2424107, 2424108,

2424109. Copies of the data can be obtained free of charge *via* https://www.ccdc.cam.ac.uk/structures/. All other relevant data generated an analyzed during this study, which include experimental, spectroscopic, crystallographic and computational data, are available within the paper and its ESI files.† Should any raw data files be needed in another format they are available from the corresponding author upon reasonable request. Source data are provided with this paper.

Author contributions

The manuscript was written through contributions of all authors. All authors have given approval to the final version of the manuscript.

Conflicts of interest

There are no conflicts to declare.

Acknowledgements

This work was supported by the National Natural Science Foundation of China (NSFC) (No. 22475018) and the Beijing Institute of Technology Research Fund Program for Young Scholars (XSQD-202211002). We thank the Analysis and Testing Centre at the Beijing Institute of Technology for advanced facilities.

References

1 (*a*) B. Peng, R. Wu and H. Li, Crystallization from a Droplet: Single-Crystalline Arrays and Heterojunctions for Organic Electronics, *Acc. Chem. Res.*, 2021, **54**, 4498–4507; (*b*) H. Jiang, S. Zhu, Z. Cui, Z. Li, Y. Liang, J. Zhu, P. Hu, H. L. Zhang and W. Hu, High-performance five-ring-fused organic semiconductors for field-effect transistors, *Chem. Soc. Rev.*, 2022, **51**, 3071–3122; (*c*) W. Jiang and Z. Wang, Molecular Carbon Imides, *J. Am. Chem. Soc.*, 2022, **144**, 14976–14991; (*d*) Y. Zhang, Y. Wang, C. Gao, Z. Ni, X. Zhang, W. Hu and H. Dong, Recent advances in n-type and ambipolar organic semiconductors and their multi-functional applications, *Chem. Soc. Rev.*, 2023, **52**, 1331–1381; (*e*) L. Ding, Z. Yu, X. Wang, Z. Yao, Y. Lu, C. Yang, J. Wang and J. Pei, Polymer Semiconductors: Synthesis, Processing, and Applications, *Chem. Rev.*, 2023, **123**, 7421–7497.

2 (*a*) M. C. Tang, M. Y. Chan and V. W. Yam, Molecular Design of Luminescent Gold(III) Emitters as Thermally Evaporable and Solution-Processable Organic Light-Emitting Device (OLED) Materials, *Chem. Rev.*, 2021, **121**, 7249–7279; (*b*) H.-H. Cho, D. G. Congrave, A. J. Gillett, S. Montanaro, H. E. Francis, V. Riesgo-Gonzalez, J. Ye, R. Chowdury, W. Zeng, M. K. Etherington, J. Royakkers, O. Millington, A. D. Bond, F. Plasser, J. M. Frost, C. P. Grey, A. Rao, R. H. Friend, N. C. Greenham and H. Bronstein, Suppression of Dexter transfer by covalent encapsulation for efficient matrix-free narrowband deep blue hyperfluorescent OLEDs, *Nat. Mater.*, 2024, **23**, 519–526.

3 (*a*) X. Zhang, X. Gu and H. Huang, Low-Cost Nonfused-Ring Electron Acceptors Enabled by Noncovalent Conformational Locks, *Acc. Chem. Res.*, 2024, **57**, 981–991; (*b*) H. Jiang, Q. Liang, H. Guo, A. Zhang, X. Wang, Z. Tang and Z. Bo, All Roads Lead to Rome: Isomers with Divergent Cathode Modification Mechanisms toward Ohmic Contact, *J. Am. Chem. Soc.*, 2024, **146**, 30262–30271; (*c*) J. Han, H. Xu, S. H. K. Paleti, A. Sharma and D. Baran, Understanding photochemical degradation mechanisms in photoactive layer materials for organic solar cells, *Chem. Soc. Rev.*, 2024, **53**, 7426–7454.

4 (*a*) N. E. Persson, P. H. Chu, M. McBride, M. Grover and E. Reichmanis, Nucleation, Growth, and Alignment of Poly(3-hexylthiophene) Nanofibers for High-Performance OFETs, *Acc. Chem. Res.*, 2017, **50**, 932–942; (*b*) H. Chen, M. Moser, S. Wang, C. Jellett, K. Thorley, G. T. Harrison, X. Jiao, M. Xiao, B. Purushothaman, M. Alsufyani, H. Bristow, S. De Wolf, N. Gasparini, A. Wadsworth, C. R. McNeill, H. Sirringhaus, S. Fabiano and I. McCulloch, Acene Ring Size Optimization in Fused Lactam Polymers Enabling High n-Type Organic Thermoelectric Performance, *J. Am. Chem. Soc.*, 2021, **143**, 260–268; (*c*) M. Li, M. Liu, F. Qi, F. R. Lin and A. K. Jen, Self-Assembled Monolayers for Interfacial Engineering in Solution-Processed Thin-Film Electronic Devices: Design, Fabrication, and Applications, *Chem. Rev.*, 2024, **124**, 2138–2204.

5 (*a*) M. Kaur and D. H. Choi, Diketopyrrolopyrrole: brilliant red pigment dye-based fluorescent probes and their applications, *Chem. Soc. Rev.*, 2015, **44**, 58–77; (*b*) M. S. Vezie, S. Few, I. Meager, G. Pieridou, B. Dorling, R. S. Ashraf, A. R. Goni, H. Bronstein, I. McCulloch, S. C. Hayes, M. Campoy-Quiles and J. Nelson, Exploring the origin of high optical absorption in conjugated polymers, *Nat. Mater.*, 2016, **15**, 746–753; (*c*) T. He, P. Leowanawat, C. Burschka, V. Stepanenko, M. Stolte and F. Wuerthner, Impact of 2-Ethylhexyl Stereoisomers on the Electrical Performance of Single-Crystal Field-Effect Transistors, *Adv. Mater.*, 2018, **30**, 201804032; (*d*) A. B. Pun, L. M. Campos and D. N. Congreve, Tunable Emission from Triplet Fusion Upconversion in Diketopyrrolopyrroles, *J. Am. Chem. Soc.*, 2019, **141**, 3777–3781; (*e*) J. A. Chiong, Y. Zheng, S. Zhang, G. Ma, Y. Wu, G. Ngaruka, Y. Lin, X. Gu and Z. Bao, Impact of Molecular Design on Degradation Lifetimes of Degradable Imine-Based Semiconducting Polymers, *J. Am. Chem. Soc.*, 2022, **144**, 3717–3726; (*f*) B. Huang, P. Chen, X. Hua, D. Qiu, T. Cui, J. Zhang, S. Zhang, C. S. Yuan, F. He, X. Shao, H. L. Zhang and Z. Liu, "Two-in-One" DPP Building Blocks for Ambipolar Conjugated Polymers in Flexible Transistors, *J. Am. Chem. Soc.*, 2025, **147**, 17954–17966.

6 (*a*) H. Chen, Y. Guo, G. Yu, Y. Zhao, J. Zhang, D. Gao, H. Liu and Y. Liu, Highly pi-extended copolymers with diketopyrrolopyrrole moieties for high-performance field-effect transistors, *Adv. Mater.*, 2012, **24**, 4618–4622; (*b*)

J. Cho, K. H. Cheon, H. Ahn, K. H. Park, S.-K. Kwon, Y.-H. Kim and D. S. Chung, High charge-carrier mobility of 2.5 cm2 V-1 s-1 from a water-borne colloid of a polymeric semiconductor *via* smart surfactant engineering, *Adv. Mater.*, 2015, **27**, 5587–5592; (*c*) J. Bai, Y. Jiang, Z. Wang, Y. Sui, Y. Deng, Y. Han and Y. Geng, Bar-Coated Organic Thin-Film Transistors with Reliable Electron Mobility Approaching 10 cm2 V-1 s-1, *Adv. Electron. Mater.*, 2020, **6**, 1901002; (*d*) Y. Pan, W. Zhang, Y. Zhou, X. Wei, H. Luo, J. Wei, L. Wang and G. Yu, Heteroatom Structural Engineering Enables Ethenylene-Bridged Bisisoindigo-Based Copolymers to Exhibit Unique n-Type Transistor Performance, *CCS Chem.*, 2024, **6**, 473–486.

7 (*a*) L. Feng, C. Li, L. Liu, X. Chen, G. Jiang, J. Wang and B. Tang, A Facile Structural Isomerization-Induced 3D Spatial D-A Interlocked Network for Achieving NIR-II Phototheranostic Agents, *Angew. Chem., Int. Ed.*, 2022, **61**, e202212673; (*b*) L. Feng, Y. Tuo, Z. Wu, W. Zhang, C. Li, B. Yang, L. Liu, J. Gong, G. Jiang, W. Hu, B. Tang, L. Wu and J. Wang, Highly Stable Near-Infrared II Luminescent Diradicaloids for Cancer Phototheranostics, *J. Am. Chem. Soc.*, 2024, **146**, 32582–32594.

8 (*a*) R. Wahalathantrige Don, P. Das, Z. Ma, U. M. Kuruppu, D. Feng, B. Shook, M. K. Gangishetty, M. C. Stefan, N. R. Pradhan and C. N. Scott, Vinyl-Flanked Diketopyrrolopyrrole Polymer/MoS2 Hybrid for Donor–Acceptor Semiconductor Photodetection, *Chem. Mater.*, 2023, **35**, 4691–4704; (*b*) L. Chen, Z. Shangguan, M. Li, G. Zhang, C. Wang and D. Zhang, High-performance vinyl-flanked diketopyrrolopyrrole–selenophene polymer semiconductors with branched, linear and cyclic alkyl side chains, *J. Mater. Chem. C*, 2024, **12**, 17050–17055; (*c*) S. Ren, S. Wang, J. Chen and Z. Yi, Design of Novel Functional Conductive Structures and Preparation of High-Hole-Mobility Polymer Transistors by Green Synthesis Using Acceptor-Donor-Acceptor Strategies, *Polymers*, 2024, **16**, 396; (*d*) Y. Wang, J. Wu, H. Guo, R. Wang, C. Xiao, P. Yang, J. Dong, L. Zhang, G. Gao and X.-H. Jin, Aryl-Ethenyl-Substituted Diketopyrrolopyrrole Semiconductors with trans Configuration and Ultraclose π-Plane Stacking Distance, *Chem. Mater.*, 2024, **36**, 4215–4225.

9 (*a*) K. V. Vinutha and R. M. Rajeswara, Vinylene-linked diketopyrrolopyrrole chromophores for electrochromism, *RSC Adv.*, 2024, **14**, 10017–10023; (*b*) Z. Zhang, F. Meng, X. Chi, Y. Jiao, B. Xue, X. Li and F. Zhang, Diketopyrrolopyrrole-Activated Dynamic Condensation Approach to Narrow-Band Gap Vinylene-Linked Covalent Organic Frameworks, *Angew. Chem., Int. Ed.*, 2024, e202417805.

10 (*a*) T. Kim, W. Kim, O. Vakuliuk, D. T. Gryko and D. Kim, Two-Step Charge Separation Passing Through the Partial Charge-Transfer State in a Molecular Dyad, *J. Am. Chem. Soc.*, 2020, **142**, 1564–1573; (*b*) J. Chen, W. Huang, D. Zheng, Z. Xie, X. Zhuang, D. Zhao, Y. Chen, N. Su, H. Chen, R. M. Pankow, Z. Gao, J. Yu, X. Guo, Y. Cheng, J. Strzalka, X. Yu, T. J. Marks and A. Facchetti, Highly stretchable organic electrochemical transistors with strain-resistant performance, *Nat. Mater.*, 2022, **21**, 564–571; (*c*) D. Zhang, C. Li, G. Zhang, J. Tian and Z. Liu, Phototunable and Photopatternable Polymer Semiconductors, *Acc. Chem. Res.*, 2024, **57**, 625–635.

11 Y. Han, Y. Xie, J. Zhang, S. Tan, H. Zhang, B. Tang, J. L. Sessler and F. Huang, Fjord-Type AIEgens Based on Inherent Through-Space Conjugation, *CCS Chem.*, 2024, **6**, 1739–1747.

12 D. Feng, G. Barton and C. N. Scott, Synthesis of 2,5-Dibutyl-3,6-dimethyl-1H,2H,4H,5H-pyrrolo[3,4-c]pyrrole-1,4-dione: A Diketopyrrolopyrrole Scaffold for the Formation of Alkenyldiketopyrrolopyrrole Compounds, *Org. Lett.*, 2019, **21**, 1973–1978.